Appl. Phys. A (2016) 122:378
DOI 10.1007/s00339-016-9855-7

Applied Physics A
Materials Science & Processing

Polarizability matrix retrieval of a non-planar chiral particle through scattering parameters

Theodosios Karamanos[1] · **Nikolaos Kantartzis**[1]

Received: 11 August 2015 / Accepted: 10 November 2015 / Published online: 14 March 2016

Abstract An efficient technique for the polarizability matrix extraction of non-planar chiral particles is introduced in this paper. Assuming electrically small sizes, the particles are modeled via electric and magnetic dipoles, whose induced moments are derived from the surface S-parameter response of three normal wave incidences. Then, these moments are inserted in the initial convention and polarizabilities are acquired through a linear system formed by the measured or simulated S-parameters. To validate the novel method, the retrieved polarizabilities are involved in RCS calculations for diverse incidences and compared with simulated ones.

1 Introduction

First-principle homogenization methods are widely acknowledged due to their consistency and accuracy. Their goal is to analytically calculate the effective constitutive parameters of bulk metamaterials [1–5] from the properties of the composing scatterers. Such an approach considers the radiation behavior of each scatterer and the interaction between scatterers on the 2D/3D grid, thus eradicating artifacts of existing algorithms, associated with weak spatial dispersion and non-locality [6].

Mainly, the prior schemes exploit single metamaterial scatterer polarizabilities. In fact, for some typical structures, polarizabilities can be analytically derived via either approximate surface current distributions [7] or antenna models [8]. However, such techniques mostly apply to certain shapes and produce quasi-static outcomes. Alternatively, generalized methods based on the scatterers' response have been lately proposed. So, apart from far-field data [9], S-paramaters (simulated or measured) constitute a popular candidate. To this aim, a dynamic technique has been presented for anisotropic scatterers [10], offering closed-form expressions for two particle polarizabilities up to the homogenization limit. Further extensions have studied simple bianisotropic metamaterials through S-parameters, raising the number of the extracted polarizabilities to four [11].

In this paper, a systematic methodology for non-planar structures with larger polarizability matrices, like the helix chiral particle, is developed. Presumed electrically small, the scatterer is described by an electric and magnetic dipole around its shape center. Next, the particles are placed in a 2D array, perpendicularly illuminated by plane wanes, and the induced dipole moments are expressed via the particle's polarizabilities and the local field at its shape center. So, a linear system is constructed and polarizabilities are derived as a function of the induced dipole moments. The latter can be obtained from simulated or measured S-parameters via equivalent surface models. The new algorithm can precisely extract the polarizability matrix of a scatterer for up to 9 elements through S-parameters and its application to the helix chiral particle. Moreover, and unlike other schemes, interaction coefficients for the 2D array are not calculated, yet extracted for simplicity. The featured method is certified by RCS computations, successfully compared to various simulated results.

✉ Nikolaos Kantartzis
kant@auth.gr

[1] Department of Electrical and Computer Engineering, Aristotle University of Thessaloniki, 54124 Thessaloníki, Greece

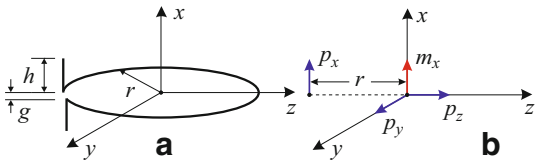

Fig. 1 Helix chiral particle. **b** Geometry with $r = 3$ mm, $h = 1$ mm, $g = 0.3$ mm, a wire radius of 0.05 mm, and the largest dimension given by $2s = 2\sqrt{r^2 + h^2}$. **b** Equivalent dipole moments and their respective positions

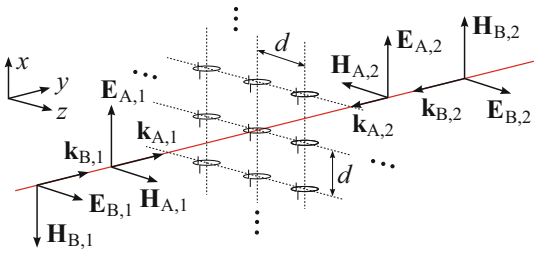

Fig. 2 Array of metamaterial scatterers ($d = 10$ mm)

2 Theoretical methodology

Consider the helix chiral particle of Fig. 1a and moderate electrical sizes, so that $|k|h < 0.3$ and $|k|r < 1$, with $k = \omega\sqrt{\varepsilon\mu}$ the wavenumber in the background medium. Thus, the particle can be deemed significantly small and represented by a set of electric and magnetic dipoles around its shape center, as in Fig. 1b. Note that, due to the non-planar geometry, not all dipole moments are located at the shape center (same position), contrary to other schemes [9–11]. Placing the scatterer on an infinite 2D array (Fig. 2), the induced electric, p, and magnetic, m, dipole moments are related to the particle polarizabilities and local fields at its center by

$$\begin{bmatrix} p_x \\ c^{-1}m_x \\ p_y \\ p_z \end{bmatrix} = \begin{bmatrix} \alpha_{\mathrm{ee}}^{xx} & \alpha_{\mathrm{em}}^{xx} & \alpha_{\mathrm{ee}}^{xy} & 0 \\ \alpha_{\mathrm{me}}^{xx} & \alpha_{\mathrm{mm}}^{xx} & \alpha_{\mathrm{me}}^{xy} & 0 \\ \alpha_{\mathrm{ee}}^{yx} & \alpha_{\mathrm{em}}^{yx} & \alpha_{\mathrm{ee}}^{yy} & 0 \\ 0 & 0 & 0 & \alpha_{\mathrm{ee}}^{zz} \end{bmatrix} \left\{ \mathbf{f}^{\mathrm{inc}} + \mathbf{f}^{\mathrm{scat}} \right\}, \tag{1a}$$

$$\mathbf{f}^{\mathrm{scat}} = \begin{bmatrix} \varepsilon_0 E_x^{\mathrm{scat}} \\ c^{-1} H_x^{\mathrm{scat}} \\ \varepsilon_0 E_y^{\mathrm{scat}} \\ \varepsilon_0 E_z^{\mathrm{scat}} \end{bmatrix} = \begin{bmatrix} C_{\mathrm{ee}}^{xx} p_x \\ C_{\mathrm{mm}}^{xx} c^{-1} m_x \\ C_{\mathrm{ee}}^{yy} p_y \\ C_{\mathrm{ee}}^{zz} p_z \end{bmatrix}, \tag{1b}$$

for α_{ee}, α_{em}, α_{mm}, and α_{me} the scatterer's electric–electric, electric–magnetic, magnetic–magnetic, and magnetic–electric polarizabilities, respectively. Vector $\mathbf{f}^{\mathrm{inc}}$ denotes the incident field and $\mathbf{f}^{\mathrm{scat}}$ the scattered one from all the other particles of the array, while their summation is the local field. Moreover, C_{ee} and C_{mm} are the electric–electric and magnetic–magnetic interaction coefficients. For the normally incident plane waves and the square array of Fig. 2, it follows that $C_{\mathrm{mm}}^{xx} = C_{\mathrm{ee}}^{yy} = C_{\mathrm{ee}}^{zz} = C_0$, according to the properties of dyadic Green's functions [12]. If the particle radius, r, is considerably smaller than the unit cell size, d, i.e., $r < 0.1$ d, it can be safely presumed that $C_{\mathrm{ee}}^{xx} \approx C_0$. Although C_0 may be analytically calculated via dyadic Green's functions, we, herein, introduce an alternative process for its extraction from S-parameters, to be next analyzed.

Since $\alpha_{\mathrm{ee}}^{zz}$ in (1) is isolated and can be separately extracted, the retrieval of the other nine elements of matrix $[\alpha]$ will, also, require nine independent equations. This is attained by plugging different incident plane waves into (1). Therefore, if $i = 1,2$ and $j = \mathrm{A}, \mathrm{B}$ indicate the direction and polarization of the incident wave, then $\mathbf{f}_{i,j}^{\mathrm{inc}} = \left[\varepsilon_0 E_x^{\mathrm{inc}} \;\; c^{-1} H_x^{\mathrm{inc}} \;\; \varepsilon_0 E_y^{\mathrm{inc}} \;\; \varepsilon_0 E_z^{\mathrm{inc}}\right]^T$ and $\mathbf{f}_{\mathrm{A},1}^{\mathrm{inc}} = \mathbf{f}_{\mathrm{A},2}^{\mathrm{inc}} = \varepsilon_0[1\ 0\ 0\ 0]^T$, $\mathbf{f}_{\mathrm{B},1}^{\mathrm{inc}} = \varepsilon_0[0\ -1\ 1\ 0]^T$, $\mathbf{f}_{\mathrm{B},2}^{\mathrm{inc}} = \varepsilon_0[0\ 1\ 1\ 0]^T$, in relation to the normally incident plane waves of Fig. 2, for normalized field values. Based on these notions, substitution of $\mathbf{f}_{i,j}^{\mathrm{inc}}$ in (1) yields

$$p_x^{\mathrm{A}} = \alpha_{\mathrm{ee}}^{xx}\left(\varepsilon_0 + C_0 p_x^{\mathrm{A}}\right) + \alpha_{\mathrm{em}}^{xx} C_0 c^{-1} m_x^{\mathrm{A}} + \alpha_{\mathrm{ee}}^{xy} C_0 p_y^{\mathrm{A}}, \tag{2a}$$

$$c^{-1} m_x^{\mathrm{A}} = \alpha_{\mathrm{me}}^{xx}\left(\varepsilon_0 + C_0 p_x^{\mathrm{A}}\right) + \alpha_{\mathrm{mm}}^{xx} C_0 c^{-1} m_x^{\mathrm{A}} + \alpha_{\mathrm{me}}^{xy} C_0 p_y^{\mathrm{A}}, \tag{2b}$$

$$p_y^{\mathrm{A}} = \alpha_{\mathrm{ee}}^{yx}\left(\varepsilon_0 + C_0 p_x^{\mathrm{A}}\right) + \alpha_{\mathrm{em}}^{yx} C_0 c^{-1} m_x^{\mathrm{A}} + \alpha_{\mathrm{ee}}^{yy} C_0 p_y^{\mathrm{A}}, \tag{2c}$$

$$p_{x,i}^{\mathrm{B}} = \alpha_{\mathrm{ee}}^{xx} C_0 p_{x,i}^{\mathrm{B}} + \alpha_{\mathrm{em}}^{xx}\left(\mp\varepsilon_0 + C_0 c^{-1} m_{x,i}^{\mathrm{B}}\right) + \alpha_{\mathrm{ee}}^{xy}\left(\varepsilon_0 + C_0 p_{y,i}^{\mathrm{B}}\right), \tag{3a}$$

$$c^{-1} m_{x,i}^{\mathrm{B}} = \alpha_{\mathrm{me}}^{xx} C_0 p_{x,i}^{\mathrm{B}} + \alpha_{\mathrm{mm}}^{xx}\left(\mp\varepsilon_0 + C_0 c^{-1} m_{x,i}^{\mathrm{B}}\right) + \alpha_{\mathrm{me}}^{xy}\left(\varepsilon_0 + C_0 p_{y,i}^{\mathrm{B}}\right), \tag{3b}$$

$$p_{y,i}^{\mathrm{B}} = \alpha_{\mathrm{ee}}^{yx} C_0 p_{x,i}^{\mathrm{B}} + \alpha_{\mathrm{em}}^{yx}\left(\mp\varepsilon_0 + C_0 c^{-1} m_{x,i}^{\mathrm{B}}\right) + \alpha_{\mathrm{ee}}^{yy}\left(\varepsilon_0 + C_0 p_{y,i}^{\mathrm{B}}\right), \tag{3c}$$

where the $\mp$ sign becomes "$-$" for the $i = 1$ incident field and "$+$" for the $i = 2$ one. Also, (2) and (3) constitute three linear systems of equations, each with three different unknowns, thus being sufficient for the desired polarizabilities. Designating as $F_{11}^{\mathrm{A}} = \varepsilon_0 + C_0 p_x^{\mathrm{A}}$, $F_{12}^{\mathrm{A}} = C_0 c^{-1} m_x^{\mathrm{A}}$, $F_{13}^{\mathrm{A}} = C_0 p_y^{\mathrm{A}}$, $F_{(i+1)1}^{\mathrm{B}} = C_0 p_{x,i}^{\mathrm{B}}$, $F_{(i+1)2}^{\mathrm{B}} = \mp\varepsilon_0 + C_0 c^{-1} m_{x,i}^{\mathrm{B}}$, and $F_{(i+1)2}^{\mathrm{B}} = \varepsilon_0 + C_0 p_{y,i}^{\mathrm{B}}$, the polarizabilities of the helix particle can be retrieved in terms of the induced dipole moments through (4).

$$\begin{bmatrix} \alpha_{\mathrm{ee}}^{xx} \\ \alpha_{\mathrm{em}}^{xx} \\ \alpha_{\mathrm{ee}}^{xy} \end{bmatrix} = [F]^{-1} \begin{bmatrix} p_x^{\mathrm{A}} \\ c^{-1} m_x^{\mathrm{A}} \\ p_y^{\mathrm{A}} \end{bmatrix}, \quad \begin{bmatrix} \alpha_{\mathrm{me}}^{xx} \\ \alpha_{\mathrm{mm}}^{xx} \\ \alpha_{\mathrm{me}}^{xy} \end{bmatrix} = [F]^{-1} \begin{bmatrix} p_{x,1}^{\mathrm{B}} \\ c^{-1} m_{x,1}^{\mathrm{B}} \\ p_{y,1}^{\mathrm{B}} \end{bmatrix},$$
$$\begin{bmatrix} \alpha_{\mathrm{ee}}^{yx} \\ \alpha_{\mathrm{em}}^{yx} \\ \alpha_{\mathrm{ee}}^{yy} \end{bmatrix} = [F]^{-1} \begin{bmatrix} p_{x,2}^{\mathrm{B}} \\ c^{-1} m_{x,2}^{\mathrm{B}} \\ p_{y,2}^{\mathrm{B}} \end{bmatrix}, \quad [F] = \begin{bmatrix} F_{11}^{\mathrm{A}} & F_{12}^{\mathrm{A}} & F_{13}^{\mathrm{A}} \\ F_{21}^{\mathrm{B}} & F_{22}^{\mathrm{B}} & F_{23}^{\mathrm{B}} \\ F_{31}^{\mathrm{B}} & F_{32}^{\mathrm{B}} & F_{33}^{\mathrm{B}} \end{bmatrix} \tag{4}$$

This new set of equations can efficiently calculate the nine unknown polarizabilities of (1), provided that the induced electric and magnetic dipole for each incidence is known. The latter may be derived from the response of the 2D array of Fig. 2, for each incidence, in the form of S-parameters or reflection/transmission coefficients, as explained below.

2.1 S-parameters from dipole moments

To evaluate the required dipole moments, the 2D array in Fig. 2 is replaced by a set of equivalent radiating surfaces. Assuming planar arrays of p_x, m_x, and p_y, the replacement involves equivalent surfaces with the respective electric and magnetic surface currents $\mathbf{J}_{sx}$, $\mathbf{K}_{sx}$, and $\mathbf{J}_{sy}$. Thus, if we follow the averaging process of [11], these surface currents can be expressed as

$$\mathbf{J}_{sx} = j\omega \frac{p_x}{d^2} \hat{\mathbf{x}}, \quad \mathbf{K}_{sx} = -j\omega\mu_0 \frac{m_x}{d^2} \hat{\mathbf{x}}, \quad \mathbf{J}_{sy} = j\omega \frac{p_y}{d^2} \hat{\mathbf{y}}. \tag{5}$$

Moreover, the appropriate boundary conditions for the surface currents of (5) lead to the scattered fields from each equivalent surface, as in Fig. 3. Gathering the scattered field contribution of each surface current, the total scattered field of the 2D array with helix particles can be obtained as a function of the dipole moments, i.e.,

$$\mathbf{E}^{\mathrm{surf}} = \mathrm{E}_x^{\mathrm{surf}} \hat{\mathbf{x}} + \mathrm{E}_y^{\mathrm{surf}} \hat{\mathbf{y}}, \tag{6a}$$

$$\mathrm{E}_x^{\mathrm{surf}} = -\frac{j\omega\eta_0}{2d^2} p_x e^{-jk(|z| \mp r)}, \tag{6b}$$

$$\mathrm{E}_y^{\mathrm{surf}} = -\frac{j\omega\eta_0}{2d^2} \left[-\mathrm{sgn}(z) c^{-1} m_x + p_y \right] e^{-jk|z|}, \tag{6c}$$

for η_0 the vacuum characteristic impedance and $\mathrm{sgn}(z)$ the sign function. Notice that in this paper, and in contrast to [9, 11], the e^{jkr} term is multiplied by the $\mathrm{E}_x^{\mathrm{surf}}$ component of (6a) to compensate for the p_x displacement from the shape center, where the local field is considered as the excitation point of the particle in (1). The $\mp$ sign in (6b) becomes "$-$" or "$+$" for a wave along the negative or positive z-axis (Fig. 3). This is analogous to the far-field calculation of an antenna array, where the distance of each element from the antenna source is signified by a phase shift at the element's own feed.

Let us, now, presume a two-port system with port 1 at the negative z-axis in Fig. 2 and port 2 at the positive one. Both ports are equally distanced from the particle, while l is the phase reference plane distance of each port from the particle shape center [11]. Then, if the distance of p_x from the reference plane of port 1, $l_x = l - r$, is set as the distance covered by the incident wave, the induced dipole moments may be computed via the acquired S-parameters, using (6) and [11], as

$$p_x^{\mathrm{A}} = \frac{j2d^2}{\omega\eta_0} \mathrm{S}_{11}^{\mathrm{A},co} e^{j2k(l-r)}, \tag{7a}$$

$$c^{-1} m_x^{\mathrm{A}} = \frac{jd^2}{\omega\eta_0} \left(\mathrm{S}_{11}^{\mathrm{A},cr} - \mathrm{S}_{21}^{\mathrm{A},cr} \right) e^{jk(2l-r)}, \tag{7b}$$

$$p_y^{\mathrm{A}} = \frac{jd^2}{\omega\eta_0} \left(\mathrm{S}_{11}^{\mathrm{A},cr} + \mathrm{S}_{21}^{\mathrm{A},cr} \right) e^{jk(2l-r)}, \tag{7c}$$

$$p_{x,1}^{\mathrm{B}} = \frac{j2d^2}{\omega\eta_0} \mathrm{S}_{11}^{\mathrm{B},cr} e^{jk(2l-r)}, \tag{8a}$$

$$c^{-1} m_{x,1}^{\mathrm{B}} = \frac{jd^2}{\omega\eta_0} \left[1 + \left(\mathrm{S}_{11}^{\mathrm{A},co} - \mathrm{S}_{21}^{\mathrm{A},co} \right) e^{j2kl} \right], \tag{8b}$$

$$p_{y,1}^{\mathrm{B}} = -\frac{jd^2}{\omega\eta_0} \left[1 - \left(\mathrm{S}_{11}^{\mathrm{A},co} + \mathrm{S}_{21}^{\mathrm{A},co} \right) e^{j2kl} \right], \tag{8c}$$

$$p_{x,2}^{\mathrm{B}} = \frac{j2d^2}{\omega\eta_0} \mathrm{S}_{22}^{\mathrm{B},cr} e^{jk(2l+r)}, \tag{9a}$$

$$c^{-1} m_{x,2}^{\mathrm{B}} = -\frac{jd^2}{\omega\eta_0} \left[1 + \left(\mathrm{S}_{22}^{\mathrm{B},co} - \mathrm{S}_{12}^{\mathrm{B},co} \right) e^{j2kl} \right], \tag{9b}$$

$$p_{y,2}^{\mathrm{B}} = -\frac{jd^2}{\omega\eta_0} \left[1 - \left(\mathrm{S}_{22}^{\mathrm{B},co} + \mathrm{S}_{12}^{\mathrm{B},co} \right) e^{j2kl} \right], \tag{9c}$$

for "co" and "cr" the co- and cross-polarization of the scattered wave relative the incident one (Fig. 2). Finally,

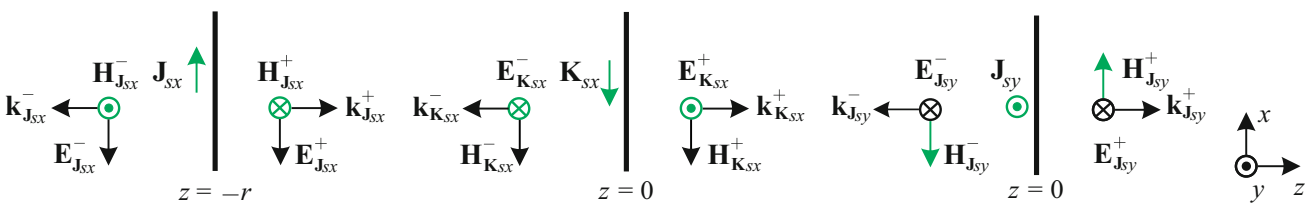

Fig. 3 Equivalent surface currents and their respective scattered fields, derived from (5) and (6), respectively. The origin of the Cartesian coordinate system is located at the shape center, while the "+" or "−" sign denotes that wave propagation occurs along the positive or negative z-axis, correspondingly

substitution of (7)–(9) in (4) leads to the desired polarizabilities. The last non-resonant polarizability a_{ee}^{zz} is retrieved simply by pivoting the particle for 90 °C and replacing x- with z-axis, to have a particle with an anisotropic behavior for waves propagating normally to the particle loop plane. Then, a_{ee}^{zz} can be computed via anisotropic polarizability extraction methods [10]. The proposed algorithm may also be applied to metamaterial scatterers with fewer polarizabilities than the helix particle and, from this viewpoint, it can comprise a generalization of the retrieval schemes in [10] and [11].

2.2 Extraction of interaction coefficient C_0

As already stated, C_0 may be determined by rapidly converging series of dyadic Green's functions. Herein, nonetheless, a simple technique, which evades the cumbersome issues of series convergence, is developed. Assume a multiply arranged random anisotropic particle, as in Fig. 2, illuminated by an incident wave $\mathbf{f}_{A,1}^{\text{inc}}$. Starting from the retrieval formulas of [10] for anisotropic scatterers (modeled by two dipoles, p_x and m_y, at their shape center) and setting C_0 as our unknown, we get

$$C_0 = \left(p_x - \alpha_{ee}^{xx}\varepsilon_0\right)/\left(p_x\alpha_{ee}^{xx}\right). \tag{10}$$

Evidently, if p_x and α_{ee}^{xx} are known, C_0 can be directly extracted from (10) for every frequency. Observe that p_x for an anisotropic scatterer may be acquired from the S-parameters of the 2D array in Fig. 2, as

$$p_x = -\frac{jd^2}{\omega\eta_0}\left(1 - \mathrm{S}_{11}^{\text{co}} + \mathrm{S}_{21}^{\text{co}}\right)e^{j2kl}, \tag{11}$$

while α_{ee}^{xx} can be analytically obtained for simple geometries. In this paper, we use the closed-form formula for the electric polarizability of a magneto-dielectric sphere [13]. So, for vaccuum as our host medium,

$$\alpha_{ee}^{xx} = 3V\frac{G(\phi)\,\varepsilon_s - \varepsilon_0}{G(\phi)\,\varepsilon_s + 2\varepsilon_0}, \tag{12a}$$

$$G(\phi) = \frac{2(\sin\phi - \phi\cos\phi)}{(\phi^2 - 1)\sin\phi - \phi\cos\phi}, \tag{12b}$$

with ε_s and μ_s the electric permittivity and magnetic permeability of the sphere, $V = 4\pi r_0^3/3$ its volume, r_0 its radius, and $\phi = \omega r_0\sqrt{\varepsilon_s\mu_s}$. Then, plugging (11) and (12) into (10) provides C_0 for a given 2D grid.

To verify our procedure, we select a dielectric sphere with $r_0 = 1.5$ mm, $\varepsilon_s = 10\varepsilon_0$, $\mu_s = \mu_0$ and compare the extracted coefficient $C_{0,\text{extr}}$ with its $C_{0,\text{calc}}$ counterpart, calculated through fast-convergence series from a popular anisotropic particle. Specifically, for the square 2D grid of Fig. 2 with $d = 10$ mm, we consider the bianisotropic split-ring resonator (BC-SRR) of the inlet sketch in Fig. 4. The latter presents the real parts of the subsequent output, retrieved via $C_{0,\text{extr}}$ and $C_{0,\text{calc}}$, which are in promising agreement. Actually, only minor resonance frequency shifts are observed, that is $\sim 0.53\,\%$ for the first magnetic resonance and $\sim 1.7\,\%$ for the second electric one. So, we, next, use $C_{0,\text{extr}}$ for our polarizability extractions to further prove its robustness.

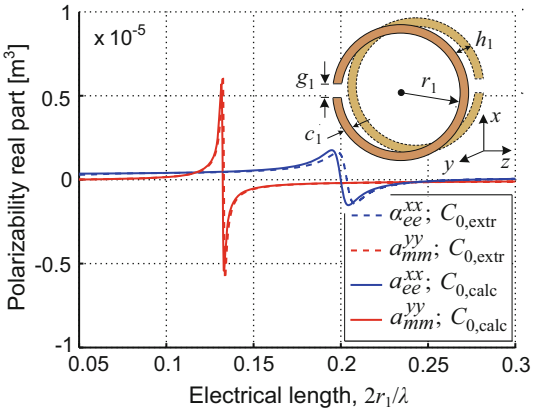

Fig. 4 Real parts of the BC-SRR polarizabilities through the extracted interaction coefficient, $C_{0,\text{extr}}$, and the calculated one, $C_{0,\text{calc}}$, for $r_1 = 3.5$ mm, $h_1 = 1.5$ mm, $c_1 = 0.25$ mm, $g_1 = 0.25$ mm, and a unit cell of $d = 10$ mm

3 Results and validation

The featured method is, now, applied to the particle of Fig. 1a, and results are given in Fig. 5, while the required S-parameter input is numerically obtained via the CST MWS™ package [14]. All results are in full qualitative accordance with previous analytical methods [8] and satisfy the Onsager–Casimir symmetries, $\overline{\overline{\alpha}}_{\text{em}} = -\overline{\overline{\alpha}}_{\text{me}}^{T}$ and $\overline{\overline{\alpha}}_{\text{ee}} = \overline{\overline{\alpha}}_{\text{ee}}^{T}$, unlike other approaches for non-planar particles [15]. This is due to the p_x phase shift in (7)–(9). Furthermore, α_{ee}^{yy} at low frequencies is equal to the non-resonant α_{ee}^{zz}, as reported [7, 8].

For their validation, the polarizabilities of Fig. 5 are, next, employed for the analytical evaluation of the particle's RCS for a given incident wave, compared with its CST MWS™ computed counterpart. In particular, if the far-field response of an electrically small particle can be described in terms of electric and magnetic dipole moments, its generated RCS is given by [16]

$$\sigma = k^4\left|(\hat{\mathbf{n}}\times\mathbf{p})\times\hat{\mathbf{n}} - (\hat{\mathbf{n}}\times c^{-1}\mathbf{m})\right|^2/(4\pi\varepsilon_0^2), \tag{13}$$

with $\hat{\mathbf{n}} = \cos\theta\,\hat{\mathbf{x}} - \sin\theta\sin\varphi\,\hat{\mathbf{y}} + \sin\theta\sin\varphi\,\hat{\mathbf{z}}$ the unit vector toward the direction of observation, as in Fig. 6. The

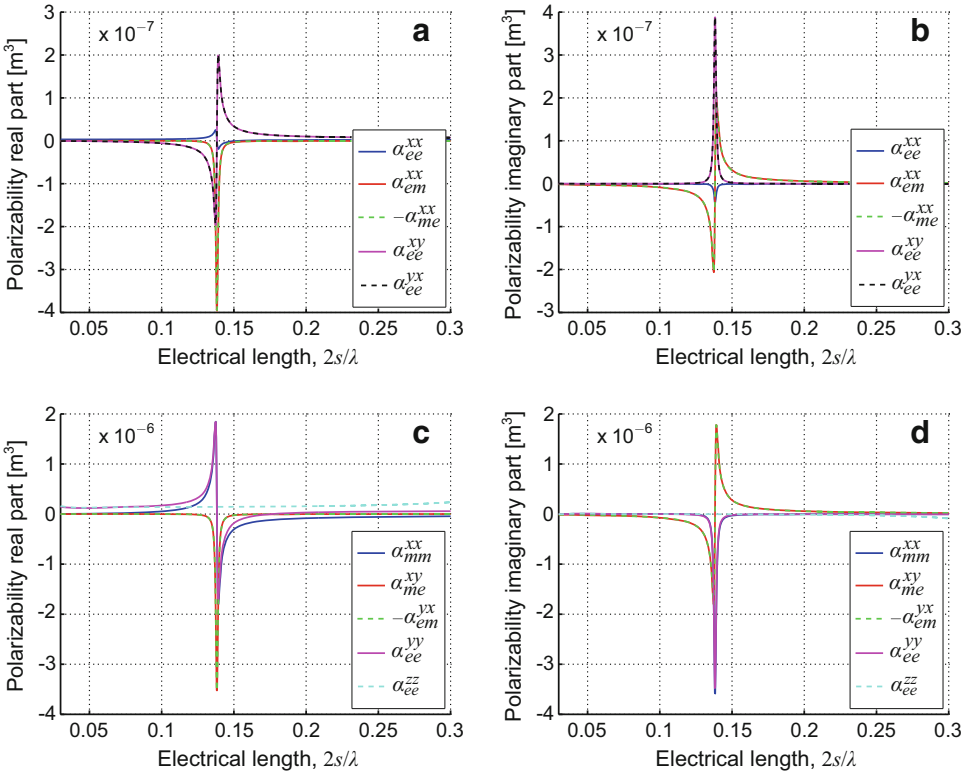

Fig. 5 Polarizabilities (real: (**a**), (**c**) and imaginary: (**b**), (**d**) part) of the helix chiral particle via the proposed method

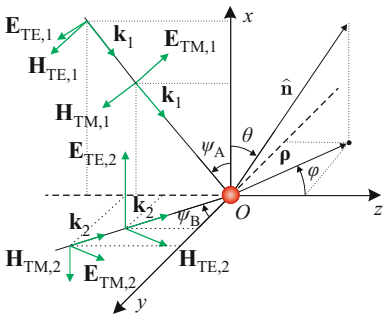

Fig. 6 The RCS calculation setup. The particle under test is placed at the axes origin O and illuminated by two TM and two TE modes with respect to the x-, y-, and z-axes

required dipole moments $\mathbf{p}$ and $\mathbf{m}$ are derived by (1), considering an isolated scatterer, i.e., $\mathbf{f}^{\text{scat}} = \mathbf{0}$.

In this way, all possible incidence angles along the four plane waves of Fig. 6 may be analyzed through normalized fields, $\mathbf{f}_{\text{inc}}^{\text{TM},1} = \varepsilon_0[\sin\psi_{\text{A}}\ 0\ 0\ \cos\psi_{\text{A}}]^T$, $\mathbf{f}_{\text{inc}}^{\text{TE},1} = \varepsilon_0[0\ -\sin\psi_{\text{A}}\ 1\ 0]^T$, $\mathbf{f}_{\text{inc}}^{\text{TM},2} = \varepsilon_0\,[0\ -1\ \sin\psi_{\text{B}}\ \cos\psi_{\text{B}}]^T$, and $\mathbf{f}_{\text{inc}}^{\text{TE},2} = \varepsilon_0[1\ 0\ 0\ 0]^T$. Nevertheless, we, herein, focus only on the $\mathbf{f}_{\text{inc}}^{\text{TM},1}$ and $\mathbf{f}_{\text{inc}}^{\text{TM},2}$ cases, since they are sufficient for the excitation of all elements of the polarizability matrix in (1). Also, five different angles of incidence, i.e., $90, 60, 45, 30,$ and 0° are investigated for ψ_{A} and ψ_{B}. Comparative plots of the calculated and simulated RCS are illustrated in Fig. 7 for the

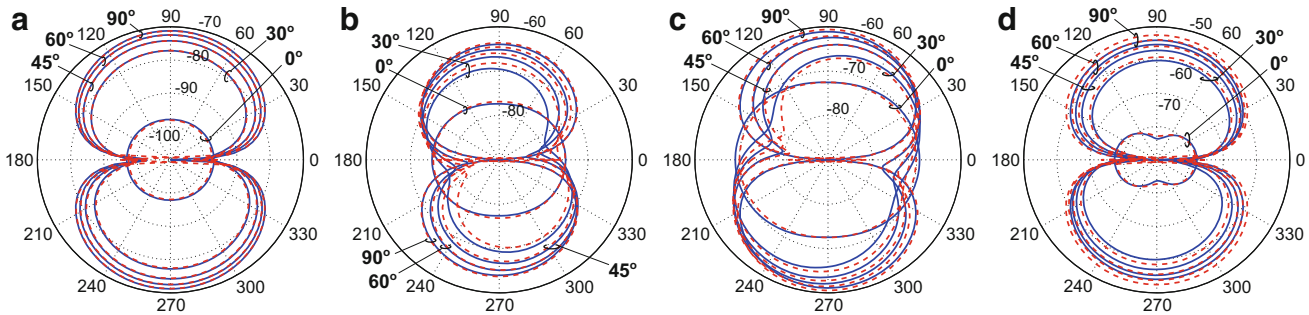

Fig. 7 Calculated (*blue solid line*) and numerically derived (*red dashed line*) polar RCS patterns of the helix chiral particle versus φ at $\theta = \pi/2$, for the TM, 1 incident plane wave in Fig. 6 and an incidence angle of ψ_{A} (*bold numbers*) at (**a**) $f = 4\,\text{GHz}$, (**b**) $f = 6\,\text{GHz}$, (**c**) $f = 7\,\text{GHz}$, and (**d**) $f = 10\,\text{GHz}$

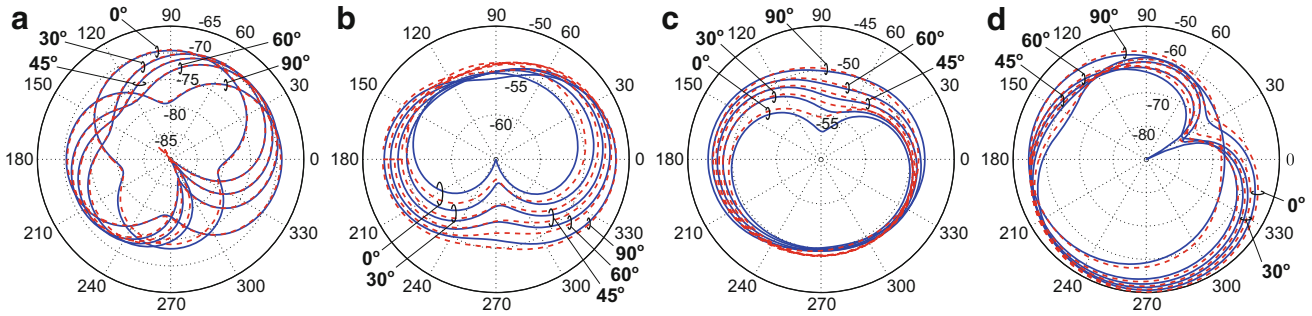

Fig. 8 Calculated (*blue solid line*) and numerically derived (*red dashed line*) polar RCS patterns of the helix chiral particle versus φ at $\theta = \pi/2$, for the TM, 2 incident plane wave in Fig. 6 and an incidence angle of ψ_B (*bold numbers*) at (**a**) $f = 4\,\text{GHz}$, (**b**) $f = 6\,\text{GHz}$, (**c**) $f = 7\,\text{GHz}$, and (**d**) $f = 10\,\text{GHz}$

TM, 1 incidence and Fig. 8 for the TM, 2 incidence. Particularly, for the low frequency $f = 4\,\text{GHz}$ scenario (electrical length of $2s/\lambda = 0.0843$), displayed in Figs. 7a and 8a, a very satisfactory match for the quasi-static response of the particle is achieved. Moving to the spectrum around the scatterer's resonance, the outcomes are shown in Figs. 7b and 8b, for $f = 6\,\text{GHz}$ ($2s/\lambda = 0.1265$), and Figs. 7c and 8c, for $f = 7\,\text{GHz}$ ($2s/\lambda = 0.1476$), respectively. Again, the agreement is undoubtedly sufficient, except for some minor deviations due to the sensitivity of polarizabilities around the resonance for small frequency shifts. Finally, Figs. 7d and 8d display the RCS results near the homogenization limit of $\lambda/5 - \lambda/4$, for $f = 10$ GHz ($2s/\lambda = 0.2108$), with similar high levels of coincidence.

Overall, the prior evaluation process substantiates the efficiency of the novel method and offers modeling guidelines for helix chiral particles or the multi-pole treatment of metamaterial structures. As shown, the dipole approximation can lead to very accurate representations of the prior particles, at least for electrical lengths around the $\lambda/5$ limit. Furthermore, the RCS obtained from the extracted polarizability matrix succeeds in following the variation of the actual RCS, both in value and in pattern, for every angle of incidence and wave polarization. This excellent agreement allows the reliable use of the extracted C_0, instead of the calculated one in relevant setups. Bear in mind, however, that the dipole approximation may not be sufficient when moderate particle dimensions are not taken into account, namely large wire lengths h. In such cases, as for electrical lengths beyond $\lambda/4$, the addition of quadrapoles in the multi-pole model is possibly required.

4 Conclusions

A rigorous algorithm for the dynamic retrieval of the polarizability matrix of non-planar helix chiral particles has been presented in this paper. Initially, it is assumed that, under certain dimensions, the helix particle can be replaced with a set of electric and magnetic dipole moments, which are, afterward, placed on a 2D square array, illuminated by normally incident plane waves. Then, the induced dipole moments of the scatterer in the array are analytically derived as a function of the polarizability matrix to form three linear systems with the unknown polarizabilities. By expressing these dipole moments in terms of the simulated or measured S-parameters, the polarizability matrix is promptly obtained. Also, a new technique for the trustworthy computation of the interaction coefficient for a 2D array has been launched. Finally, the extracted polarizabilities have been extensively certified through comparisons of the resulting RCS patterns with simulated ones, for frequencies up to the homogenization limit.

References

1. V. Yannopapas, Appl. Phys. A **87**, 259–264 (2007)
2. A. Chipouline, J. Petschulat, A. Tuennermann, T. Pertsch, C. Menzel, C. Rockstuhl, F. Lederer, Appl. Phys. A **103**, 899–904 (2011)
3. A. Alù, Phys. Rev. B **84**, 075153 (2011)
4. M.H. Belyamoun, O. Dubrunfaut, S. Zouhdi, Appl. Phys. A **109**, 1043–1051 (2012)
5. T.D. Karamanos, S.D. Assimonis, A.I. Dimitriadis, N.V. Kantartzis, Photon. Nanostruct. Fundam. Appl. **12**, 291–297 (2014)
6. T. Koschny, P. Markoš, D.R. Smith, C.M. Soukoulis, Phys. Rev. E **68**, 065602(R) (2003)
7. R. Marqués, F. Mesa, J. Martel, F. Medina, IEEE Trans. Antennas Propag. **51**, 2572–2581 (2003)
8. S.A. Tretyakov, F. Mariotte, C.R. Simovski, T.G. Kharina, J.-P. Heliot, IEEE Trans. Antennas Propag. **44**, 1006–1014 (1996)
9. V.S. Asadchy, I.A. Faniayeu, Y. Radi, S.A. Tretyakov, Photon. Nanostruct. Fundam. Appl. **12**, 298–304 (2014)
10. A.D. Scher, E.F. Kuester, Metamaterials **3**, 44–55 (2009)
11. T.D. Karamanos, A.I. Dimitriadis, N.V. Kantartzis, IET Mocrow. Antennas Propag. **8**, 1398–1407 (2014)
12. P.A. Belov, C.R. Simovski, Phys. Rev. E **72**, 026615 (2005)
13. C.L. Holloway, E.F. Kuester, J. Baker-Jarvis, P. Kabos, IEEE Trans. Antennas Propag. **51**, 2596–2603 (2003)

14. CST MWS^{TM}: Computer Simulation Technology: Microwave Studio, CST Std. (2014)
15. T.D. Karamanos, N.V. Kantartzis, in Proceedings of the 8th International Congress on Advanced Electromagnetic Materials in Microwaves and Optics (Copenhagen, 2014) pp. 154–156
16. J.D. Jackson, *Classical Electrodynamics*, 3rd edn. (Wiley, New York, 1999)